Low-Temperature Kinetics of Reactions of the OH Radical with Propene and 1-Butene Studied by a Pulsed Laval Nozzle Apparatus Combined with Laser-Induced Fluorescence

Andrei B. Vakhtin, Seonkyung Lee, Dwayne E. Heard,† Ian W. M. Smith,† and Stephen R. Leone*

JILA, National Institute of Standards and Technology and University of Colorado, and Department of Chemistry and Biochemistry, University of Colorado, Boulder, Colorado 80309-0440

Received: March 1, 2001; In Final Form: May 7, 2001

The kinetics of the reactions of the OH radical with propene and 1-butene are studied at $T = 103$ K. The low-temperature environment is provided by a pulsed Laval nozzle supersonic expansion of nitrogen with admixed radical precursor and reactant gases. The gas number density and temperature distributions in the flow are characterized by both dynamic pressure measurements and laser-induced fluorescence (LIF) spectroscopy of OH radicals excited in the (1,0) band of the $A^2\Sigma^+ - X^2\Pi_i$ transition. For the kinetic measurements, the OH radical decay profiles in the presence of reactants are monitored by LIF. The rate constants of the reactions of OH with propylene and 1-butene are measured at $T = 103$ K to be $(0.81 \pm 0.18) \times 10^{-10}$ and $(1.24 \pm 0.27) \times 10^{-10}$ cm^3 molecule^{-1} s^{-1}, respectively. The observed negative temperature dependences of the rate constants for both reactions studied by the pulsed Laval nozzle system show good agreement with both low-temperature and high-temperature kinetic data available in the literature.

Introduction

Low temperature gas-phase kinetics have attracted growing interest in the past decade. Attention to this relatively new field is due to its importance for both practical and fundamental reasons. Obvious applications involve the atmospheric chemistry of Earth, as well as that of other planets and their moons, and the chemistry which leads to the formation of molecules in dense interstellar clouds. In modeling the processes occurring in all of these low-temperature environments, researchers generally still have to extrapolate the high-temperature kinetic data for elementary reactions (obtained typically at temperatures of 300 K and higher) to lower temperatures. However, recent low-temperature kinetic measurements involving the use of cryogenically cooled reaction cells and supersonic flow apparatuses have shown that such extrapolations can lead to significant errors.[1] For many neutral−neutral reactions studied, the rate constants exhibit essentially non-Arrhenius behavior at low temperatures, challenging both experimentalists and theoreticians to understand the mechanisms involved. The fundamental aspects of low-temperature kinetics include, in particular, the effect of long-range electrostatic interactions on the reaction rates, kinetic isotope effects, and the role of quantum tunneling in reaction dynamics.

There are two main techniques for low-temperature kinetic measurements: cryogenic cooling of the reaction cell and generating the low-temperature environment using a supersonic expansion of gas. The first method, which has been successfully used for a number of reactions down to, or close to, the temperature of liquid nitrogen,[1−8] has intrinsic limitations associated with reagent gas condensation and technical difficulties in maintaining very low temperatures by cryogenic cooling of the cell.[1] Alternative methods utilize a supersonic expansion for cooling of the gas. In 1984, Rowe and co-workers showed that supersonic expansions through Laval nozzles can generate gas flows with uniform temperature and density, which can then be used as a wall-free reactor for low-temperature kinetic studies of ion−molecule reactions.[9,10] The technique was subsequently successfully applied to studying neutral−neutral reactions.[11,12] In contrast to the cryogenic cell, the Laval nozzle technique is much less affected by the problems associated with gas condensation and it is capable of producing very low-temperature environments (down to 7 K).[13] During the last several years, dozens of rate constants of ion−molecule and neutral−neutral reactions were measured in the temperature range of 7−300 K in the two existing, continuous flow, CRESU (Cinétique de Réaction en Ecoulement Supersonique Uniforme) apparatuses[13] in Rennes and Birmingham. These CRESU experiments involve a continuous collimated supersonic flow, which provides a well-defined low-temperature environment. However, to provide a background pressure that is low enough for the supersonic flow to exist, enormous pumping capacity is required. To avoid this problem, a pulsed Laval nozzle apparatus has also been developed by the group of M. A. Smith.[14] Due to the relatively low duty cycle of the pulsed nozzle operation, only a modest pumping capacity is necessary. A pulsed Laval nozzle apparatus coupled with laser-induced fluorescence has been successfully used by M. A. Smith's group in Arizona to measure the low-temperature rate constants of the reactions of OH radicals with NO[14,15] and HBr.[16]

A similar pulsed Laval nozzle apparatus has been built in our group at JILA. M. A. Smith et al. used a pulsed cold cathode discharge to produce radicals, whereas our apparatus is designed to allow photolytic generation of transient species. Both optical and mass-spectrometric methods can be employed for diagnostics. In previous publications of the JILA group,[17−19] it was demonstrated that the pulsed Laval nozzle can provide a

* Corresponding author and staff member, Quantum Physics Division, National Institute of Standards and Technology.

† JILA Visiting Fellow; permanent address: D. E. Heard, School of Chemistry, University of Leeds, Leeds, LS2 9JT, U.K.; I. W. M. Smith, School of Chemistry, The University of Birmingham, Edgbaston, Birmingham B15 2TT, U.K.

10.1021/jp010809d CCC: $20.00
Published on Web 07/26/2001

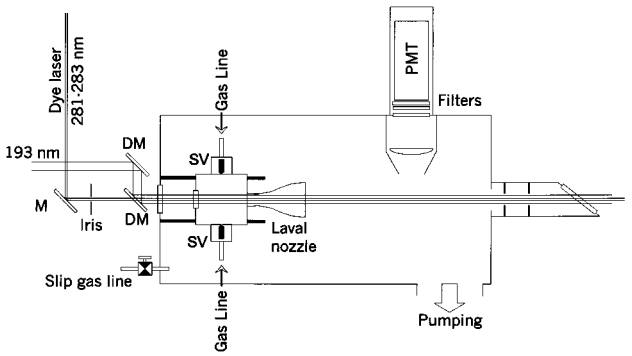

Figure 1. Schematic of the pulsed Laval nozzle apparatus. PMT is a photomultiplier tube, SV are solenoid valves, DM are dielectric mirrors with maximum reflectivity for 193 nm at 45° incidence angle, *M* is a steering mirror (or quartz plate) for the dye laser beam.

collimated supersonic flow, and preliminary results were reported on the rate constants of C_2H radicals with O_2 and C_2H_2 in the temperature range of 90−120 K by using single-photon ionization time-of-flight mass-spectrometry. However, those preliminary results on C_2H kinetics showed poor agreement with the data reported by other groups. The low-temperature kinetic results on the OH + HBr reactions reported by the Sims et al.[20] (continuous Laval expansion) and Atkinson et al.[16] (pulsed Laval expansion) are also not in a very good agreement. Therefore, more evidence has to be presented to prove the capabilities of the pulsed Laval method, i.e., a careful characterization of the pulsed supersonic flow must be performed, and reference reactions that allow comparison with other low-temperature data are needed.

In the present paper, we report our data on the detailed characterization of the pulsed Laval supersonic flow, which involve both dynamic pressure measurements and laser-induced fluorescence (LIF) spectroscopy to characterize the rotational temperature of OH. We have also measured the rate constants of the reactions of OH radicals with propene (C_3H_6) and 1-butene (C_4H_8)

$$OH + C_3H_6 \xrightarrow{k_1} \text{products} \qquad \text{(R1)}$$

$$OH + C_4H_8 \xrightarrow{k_2} \text{products} \qquad \text{(R2)}$$

at $T = 103$ K. These reactions proceed mainly by addition of the radical to the alkene to produce hydroxy alkyl radicals. Despite the low total pressure in our experiments, the temperature is low enough and the product radicals large enough for these association reactions to be at, or very close to, their high pressure limits. Reactions (R1) and (R2) are relatively fast, their rate constants showing apparent negative temperature dependences.[21−23] Moreover, for reaction (R2), low-temperature kinetic data from the continuous Laval nozzle apparatus are available;[24] thus comparison with current data can be used as a benchmark for testing the performance of the pulsed Laval nozzle experimental apparatus and procedures.

Experimental Section

The apparatus used in this work is generally similar to that described in the previous publications of this group.[17] However, certain modifications, in particular, the arrangements for LIF measurements are made. The LIF technique is used both to measure the temperature in the flow and to study the kinetics of OH radical reactions. Figure 1 shows the schematic of the experimental setup. A detailed description of the Laval nozzle block and the chamber have been presented earlier,[17] so only a brief outline of this part is presented here. The Laval nozzle block is mounted inside a stainless steel chamber. The nozzle block can be translated for about 30 cm along the chamber axis. Two pulsed solenoid valves supply an ∼5 ms gas pulse (nitrogen with admixed radical precursor and reactant gases) to the preexpansion chamber of the nozzle block. The gas expands through the Laval nozzle to the chamber pumped by a mechanical pump (60 L/s). The expansion results in a collimated supersonic gas flow, which is characterized by a uniform Mach number, gas number density, and temperature along the flow axis for 10−20 cm. In the present work, a Laval nozzle designed for a Mach number $M = 3$ expansion is used. Two differential pressure transducers (not shown in Figure 1) are used to characterize the expansion. The first one measures the stagnation pressure in the preexpansion chamber. The second pressure transducer, which can be moved across the flow downstream of the nozzle, measures the dynamic pressure in the supersonic flow. The background pressure in the chamber is measured by a capacitance manometer. An additional gas line could be used to supply a slip gas (helium) to the chamber in order to match the background pressure to the static flow pressure to achieve optimal collimation of the flow. Fortunately, for the Laval nozzle used in this work, the capacity of the pump provides the background pressure that exactly matches the conditions for the best collimation of the flow. Therefore, no slip gas is used.

The chamber and the nozzle block have quartz windows, which makes it possible to introduce laser beams along the axis of the gas flow to generate radicals photolytically (an excimer laser) and for laser-based techniques for diagnostics (tunable frequency-doubled dye laser). In this work, LIF from OH is used as a probe. The output flange of the chamber is equipped with a baffle arm ending with a quartz Brewster angle window to minimize the scattered light.

The OH radicals are produced by the reaction of $O(^1D)$ atoms with *n*-butane and also by direct photolysis of H_2O_2. The $O(^1D)$ atoms are generated by pulsed photolysis of N_2O at 193 nm (ArF excimer laser). When H_2O_2 is used as the OH radical precursor, the excimer laser is switched to 248 nm (KrF). An unfocused or slightly focused (with a quartz lens of ∼200 cm focal length) beam from the excimer laser, producing up to 70 mJ/pulse at a repetition rate of 10 Hz, is used for photolysis.

The frequency-doubled output radiation of a pulsed dye laser operating on Rhodamine 690 dye and pumped by the second harmonic of a Nd:YAG laser is used for excitation of LIF in the (1,0) band of the $A^2\Sigma^+ - X^2\Pi_i$ transition of OH (excitation wavelength range ≈ 281−283 nm). The arrangement of the optical elements used for steering and alignment of the two laser beams is shown in Figure 1. An iris aperture is used to restrict the diameter of the dye laser probe beam to 3 mm, which is considerably smaller than the diameter of the unfocused beam of the excimer laser (which is ∼1 cm in the supersonic flow region). No focusing of the dye laser beam is used. LIF from OH is detected in the (1,1) and (0,0) bands of the A−X transition by a photomultiplier (PM) tube equipped with an UG-11 UV-band-pass filter and a narrow-band interference filter (310 ± 10 nm). The PM mounted 15 cm downstream of the nozzle detects the light that is collected by a quartz lens (5 cm in diameter and 5 cm focal length). The lens focuses the image of the segment of the irradiated zone, which is about 2 cm long, to the PM photocathode. The optics are appropriately shielded to minimize the effect of the scattered light.

For the kinetic experiments, the probe laser is tuned to the $Q_1(1)$ line of the OH (1,0) band, and the signal from the photomultiplier is averaged using a boxcar integrator (10 s time constant, 200 ns gate width, 200 ns delay with respect to the excitation laser pulse). The kinetics of the OH decay are traced by monitoring the OH LIF intensity vs delay between the photolysis and probe laser pulses. Typically, for each delay time, the signal is averaged over 10−100 laser pulses. The triggering of all units and devices is provided by a four-channel digital delay/pulse generator.

LIF excitation spectra of OH are also used to measure the temperature in the supersonic flow by fitting the observed rotational distributions to a Boltzmann function. In recording the LIF spectra, the PM signal is transferred to a digital oscilloscope interfaced to a computer, which is used for the data acquisition and for controlling the wavelength of the dye laser. The signal is averaged over 10 pulses for each wavelength. In recording the LIF excitation spectra, the probe laser pulse energy is considerably reduced by replacing one of the steering mirrors (shown as M in Figure 1) by a thin quartz plate, to ensure that the spectra are obtained in the linear regime. It has been checked that, even for the strongest OH absorption lines, the LIF intensity is linear with dye laser pulse energy.

The gas flows, supplied from cylinders through stainless steel lines and controlled by a block of five mass flow controllers, are mixed in a 150 cm^3 stainless steel cylinder on their way to the nozzle block. In the experiments involving the H_2O_2 photolysis, a controlled flow of N_2 is bubbled through a sample of a concentrated (>90%) aqueous solution of hydrogen peroxide and then mixed into the main flow of the carrier gas. The total gas number density in the collimated supersonic flow is calculated using the measured background pressure in the chamber (which should be equal to the flow static pressure). The gas density obtained in this way is in very good agreement with that derived from the dynamic pressure measurements by using the Rayleigh formula combined with the isentropic relations (eqs (1−4), see Results and Discussion). The gas number densities for individual components are calculated from the total density and the known relative mass flows. The flow controllers are calibrated for individual gases by measuring the rate of filling a known volume.

Some spectroscopic and kinetic experiments are also performed at room temperature. In these measurements, a gas mixture containing N_2, radical precursor, and reactant is admitted continuously to the chamber through a special gas inlet port, bypassing the Laval nozzle block. The desired constant pressure in the chamber is maintained by adjusting the conductance of the valve connecting the chamber to a mechanical pump.

The gases used are as follows: N_2 (99.999%), N_2O (99.9995%), *n*-butane (99.9%), propene (99.6%), 1-butene (99%). All the gases are used as supplied without purification.

Results and Discussion

Characterization of the Supersonic Flow. To characterize the temperature, pressure, and gas density in the supersonic flow produced by the Mach 3 Laval nozzle, we used dynamic pressure measurements and laser-induced fluorescence spectroscopy of OH.

The procedure for the characterization of the supersonic flow produced by the Laval nozzle by dynamic pressure measurements was described in detail earlier.[17] Briefly, the stagnation pressure P_0 in the preexpansion region and the dynamic pressure P_i downstream of the nozzle on the flow axis are measured. For isentropic flow, the Rayleigh formula gives the following relationships between P_0 and P_i

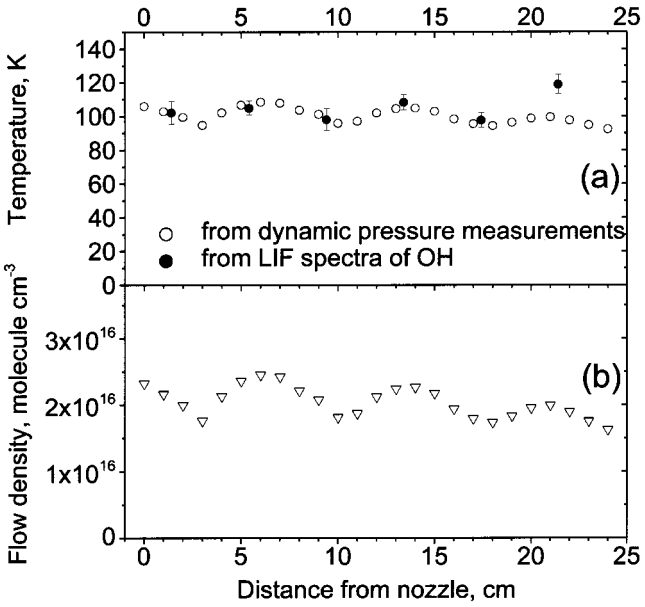

Figure 2. Profiles of temperature (a) and density (b) in the supersonic flow produced by the Mach 3 Laval nozzle. Open points: dynamic pressure measurements; filled points: temperatures derived from the LIF spectra of the OH radical.

$$\frac{P_i}{P_0} = \left[\frac{(\gamma+1)M^2}{(\gamma-1)M^2+2}\right]^{\frac{\gamma}{\gamma-1}}\left[\frac{\gamma+1}{2\gamma M^2-\gamma+1}\right]^{\frac{1}{\gamma-1}} \quad (1)$$

where M is the Mach number and γ is the ratio of specific heat capacities (C_p/C_v). Pressure and density in the flow are related to temperature through the isentropic relations

$$\frac{T_0}{T_f} = 1 + \frac{\gamma-1}{2}M^2 \quad (2)$$

$$\frac{P_0}{P_f} = \left(\frac{T_0}{T_f}\right)^{\frac{\gamma}{\gamma-1}} \quad (3)$$

$$\frac{\rho_0}{\rho_f} = \left(\frac{T_0}{T_f}\right)^{\frac{1}{\gamma-1}} \quad (4)$$

where T_0, P_0, ρ_0, and T_f, P_f, ρ_f are the temperature, pressure, and density in the stagnation region and in the flow, respectively.

Figure 2 shows the temperature, pressure and density profiles of the flow produced by the Mach 3 nozzle, obtained from the dynamic pressure measurements. The actual Mach number of the nozzle is found to be $M = 3.12 \pm 0.15$. It follows from the dynamic pressure measurements that the expansion produces a flow that is characterized by a temperature of $T = 101 \pm 7$ K, gas number density of $(2.06 \pm 0.34) \times 10^{16}$ molecules cm^{-3}, and a flow pressure of 0.22 ± 0.05 Torr (29 ± 7 Pa). It is seen from Figure 2 that there are certain oscillations of the flow parameters as a function of distance from the nozzle; these are probably caused by the nonideality of the nozzle and are difficult to avoid entirely. Because the oscillations of the gas density and temperature will affect the accuracy of the kinetic measurements, they are included when reporting the uncertainties of the measured rate constants.

Analysis of the rotational distributions of the OH radical is used as an independent means for characterizing the temperature in the supersonic flow. Figure 3(a) shows the LIF spectra of

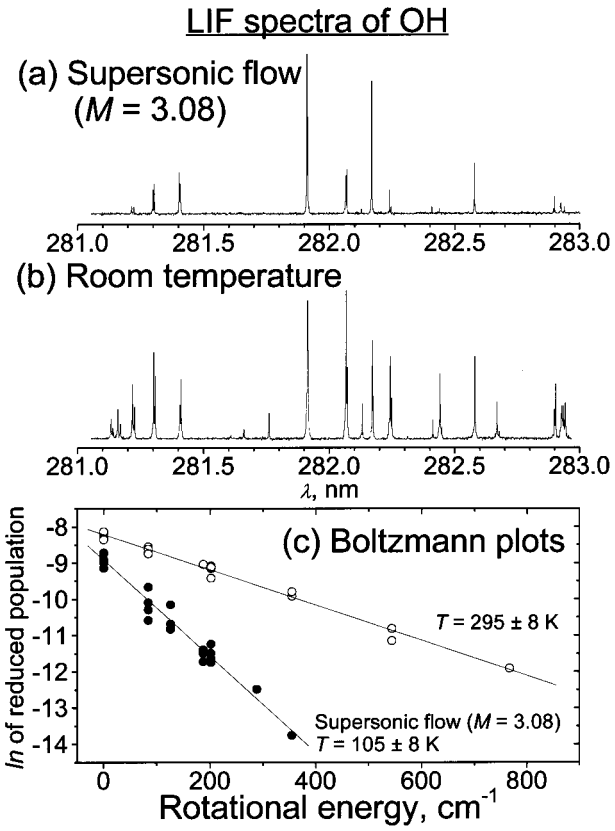

Figure 3. Examples of the LIF spectra of OH obtained in the supersonic flow produced by the Mach 3 Laval nozzle (a) and at room temperature (b). The temperatures are derived from the gradients of the corresponding Boltzmann plots (c).

OH formed in the supersonic flow produced by the Laval nozzle (for comparison, a room-temperature spectrum is shown in Figure 3b). In recording the spectra, the probe laser power was significantly reduced to avoid saturation of OH absorption (see Experimental Section). The delay between the photolysis and the probe laser pulses is set at 5 μs. It was checked that this delay is sufficient to provide appropriate conversion of the $O(^1D)$ atoms, produced by the photolysis of N_2O, to OH as well as rotational thermalization of the OH. The spectrum obtained in the supersonic flow is much simpler than the room-temperature spectrum, which is indicative of the lower temperature achieved in the expansion through the Laval nozzle. To derive the temperatures from the spectra, the natural logarithms of intensities of each individual line divided by the degeneracy of the lower level and the appropriate Einstein *B* coefficient are plotted against the energy of the lower rotational level. The line intensities are obtained by integrating the individual line profiles. The Einstein *B* coefficients for individual vibronic transitions and the rotational terms of the $X^2\Pi_i$ and $A^2\Sigma^+$ states of OH are taken from the papers by Chidsey and Crosley[25] and Coxon,[26] respectively. Figure 3c shows examples of the Boltzmann plots obtained at room temperature and in the supersonic flow. The slopes of the straight lines that fit the experimental points give temperatures of 295 and 105 K, respectively. The filled points in Figure 2a show the temperature profile along the axis of the supersonic flow measured by LIF. In these experiments, the temperatures are extracted from the spectra recorded at different distances between the nozzle and the PM detection region approximately in the middle of the gas pulse (corresponding to a 4.5 ms delay time in Figure 4 showing the gas pulse profile).

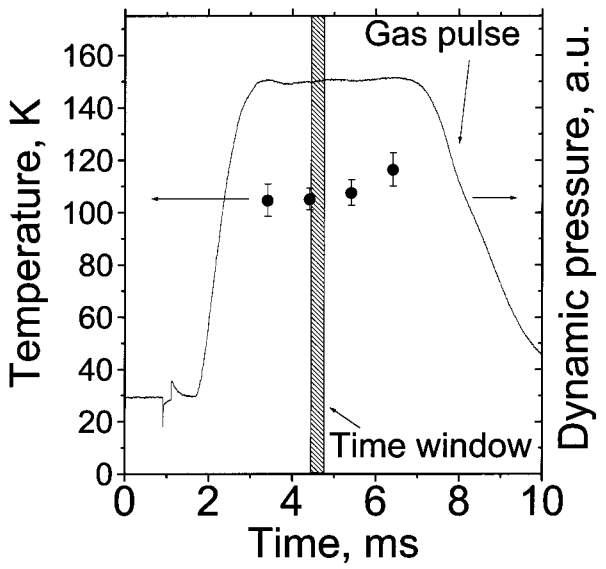

Figure 4. Temperature distribution (measured by LIF) along the gas pulse profile. The time window available for kinetic measurements is shown as the shaded area.

Two other checks were made. First, the temperatures were derived separately from the spectral lines corresponding to the two spin−orbit components of the $X^2\Pi_i$ state of OH. No systematic variations in calculated temperatures were observed. Second, the temperature profile across the 5 ms gas pulse was recorded at a fixed nozzle-PMT distance (5.4 cm). The experiments show that the temperature is uniform at least within 2 ms during the central portion of the gas pulse (see Figure 4). Note that only a very small part of the gas pulse is actually used in the kinetic measurements because the photolysis laser pulse irradiates only a column of the flow that is several tens of centimeters long, which corresponds to a time window of several hundred microseconds, typically 200−300 μs (see Figure 4). Therefore, the two-millisecond region of uniform temperature is more than enough for kinetic studies.

In conclusion, the results of the temperature measurements obtained by the two methods agree very well. The temperature is uniform within ~20 cm downstream of the nozzle and can be expressed as $T = 103 \pm 9$ K. For the supersonic flow characterized by $M = 3.1$, this distance corresponds to an ~300 μs time window available for kinetic measurements. The above results confirm that the pulsed Laval nozzle apparatus provides an acceptable low-temperature environment for kinetic studies.

Rate Constants for the OH + Propene and OH + 1-Butene Reactions at $T = 103$ K. The rate constants of the reactions of the OH radicals with propene and 1-butene, (R1) and (R2), were measured at 103 K using the pulsed Laval nozzle expansion method and LIF detection of the disappearance of the OH radicals. Reactions (R1) and (R2) are good candidates to begin a study of the kinetics of OH, since they are expected to be fast even at $T = 103$ K,[21−24] which is important in view of the limited time window (≤300 μs) available for detection of the OH temporal decay.

First, we attempted to use the $O(^1D) + n\text{-}C_4H_{10}$ source of OH radical for measurements of the rate constants. However, this method of OH production turned out to be unsuitable for kinetic studies under our experimental conditions. For the OH kinetic profiles, an instant rise of the OH LIF signal just after the photolysis pulse was followed by a much slower increase and subsequent decay of OH with time, with the shape of both

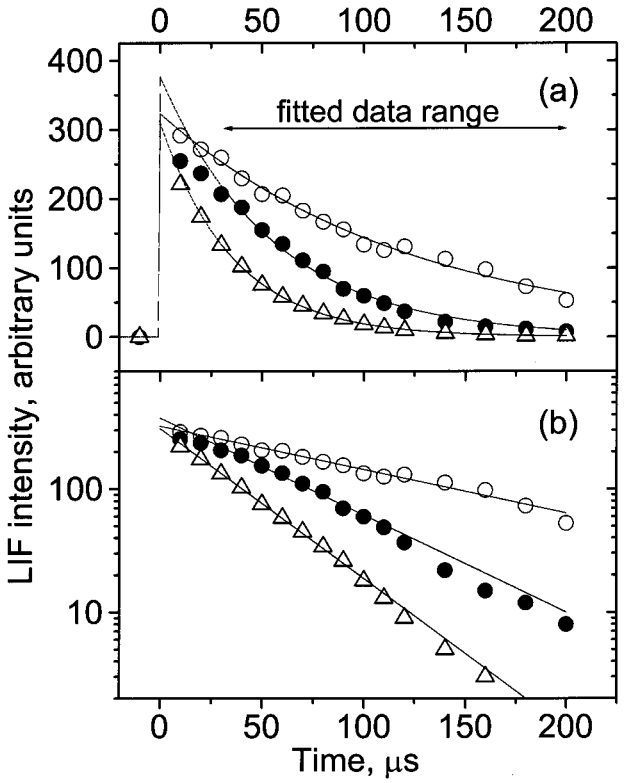

Figure 5. Representative examples of the OH decay profiles obtained at different propene concentrations (○, 4.8×10^{13} molecules cm^{-3}; ●, 1.5×10^{14} molecules cm^{-3}; △, 2.8×10^{14} molecules cm^{-3}) plotted in normal (a) and semilogarithmic (b) coordinates. The OH radicals were generated by photolysis of H_2O_2 at 248 nm.

the rising and decaying parts of the kinetic curves being dependent on the reactant (propene or 1-butene) concentration. It was possible to extract the OH decay times from the tails of the kinetic curves; moreover, the reciprocals of those times showed reasonable linearity with reactant concentration. However, the interference of the rising part of the kinetic profiles indicated some additional processes were superimposed on the OH reactive decay. The most important of these unwanted processes is probably the formation of OH($v = 0$) through collisional relaxation of vibrationally excited OH (which is very likely to be formed in the $O(^1D) + n\text{-}C_4H_{10}$ reaction).[27,28] If the OH reactive decay is complicated by additional sequential stages of relaxation, it is unclear whether reaction or relaxation determines the apparent decay time extracted from the tail of the overall kinetic curve. In view of this ambiguity, it was decided to use 248 nm photolysis of H_2O_2 as a source of OH for kinetic purposes. Photolysis of H_2O_2 at 248 and 266 nm is known to be a clean source of vibrationally cold OH;[29,30] the quantum yield of OH production is close to 2, according to the recommendations of Atkinson et al.[31]

Figure 5 shows representative examples of OH decay profiles obtained at different concentrations of propene, with H_2O_2 photolysis used as the source of OH radicals. Similar results have been obtained for OH decay kinetics in the presence of 1-butene. For both reactions (R1) and (R2), the kinetic curves are well described by a single-exponential decay function. Significant deviations from single-exponential behavior were observed only for the early stages of the decay, where rotational relaxation effects are likely to be important.[32,24] Therefore, in the fitting procedure, we neglect the first two points of the experimental kinetic curves, i.e., we fit only the tails of the OH time profiles, starting at 30 μs delay between the

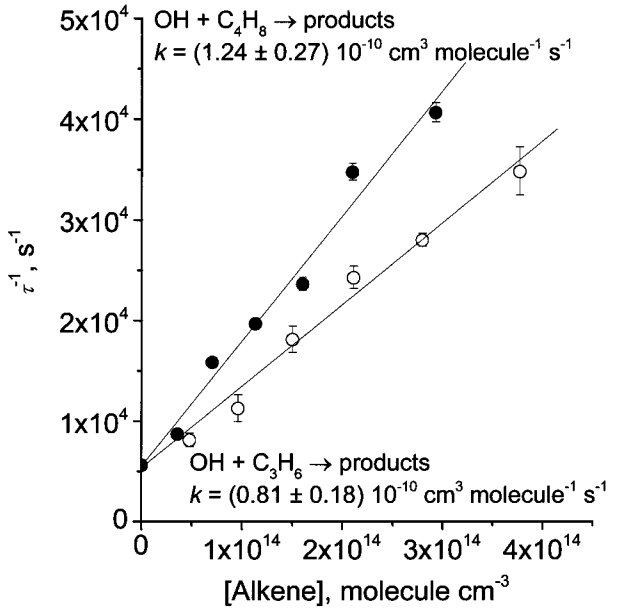

Figure 6. Reciprocal OH decay time vs reactant concentration plotted for OH + C_3H_6 (open circles) and OH + C_4H_8 (filled circles) reactions. For each concentration, the error bars indicate two standard deviations of the fit of the experimental kinetic curves by a single-exponential function. The lines show the $1/\sigma^2$-weighted linear fits.

photolysis and the probe laser pulses (the fitted data range is shown by the horizontal arrow in Figure 5). The pseudo-first-order plots for reactions (R1) and (R2) are shown in Figure 6. The corresponding rate constants, obtained from the slopes of the straight lines that fit the experimental dependences, are as follows

$$k_1 = (0.81 \pm 0.18) \times 10^{-10}\ \text{cm}^3\ \text{molecule}^{-1}\ \text{s}^{-1}$$

$$k_2 = (1.24 \pm 0.27) \times 10^{-10}\ \text{cm}^3\ \text{molecule}^{-1}\ \text{s}^{-1}$$

The intercept can probably be explained by the loss of the OH radicals due to diffusion from the zone irradiated by the photolysis laser beam and the reaction of OH with H_2O_2 ($k = 1.4 \times 10^{-12}$ cm^3 $molecule^{-1}$ s^{-1} at room-temperature).[33] The indicated uncertainties of k_1 and k_2 include both the statistical errors and the uncertainty associated with the inhomogeneity of the gas density profile along the flow axis (see Figure 2b). The latter was treated as a "component of uncertainty arising from a systematic effect"[34] and was assumed to have a rectangular probability distribution. The corresponding value of σ was obtained by dividing half of the interval between the upper and lower limits by $\sqrt{3}$.[34] Then the "combined standard uncertainty" values σ_c were calculated using the root-sum-of-squares method. In this work the uncertainties of the measured rate constants are reported as $2\sigma_c$. The details of the experimental conditions are presented in Table 1. It is noteworthy that the values of k_1 and k_2 obtained in these experiments are essentially the same as those derived from the kinetic curves with the $O(^1D)$/*n*-butane OH radical source (see above).

Figure 7 shows the rate constants k_1 and k_2 measured in this work, together with the literature data plotted as a function of temperature. For the OH + 1-butene reaction, the rate constant measured in this work agrees well with the only available low-temperature data set.[24] Moreover, for both (R1) and (R2), there is also very good consistency between the low-temperature data and those at room temperature and above, if one plots the Arrhenius expressions for the high-pressure rate constants

TABLE 1: Rate Constants for the Reactions of OH Radical with Propene (k_1) and 1-Butene (k_2) Measured at $T = 103 \pm 9$ K

reaction	carrier gas	total gas density, molecule cm^{-3}	[Alkene], molecule cm^{-3}	rate constant*, cm^3 molecule^{-1} s^{-1}
OH + propene	N_2	2.1×10^{16}	$(0.48-3.8) \times 10^{14}$	$(0.81 \pm 0.18) \times 10^{-10}$
OH + 1-butene	N_2	2.1×10^{16}	$(0.36-2.9) \times 10^{14}$	$(1.24 \pm 0.27) \times 10^{-10}$

* The indicated uncertainties are represented as $\pm 2\sigma_c$, where σ_c is a "combined standard uncertainty" that accumulates both statistical and systematic errors (see text).

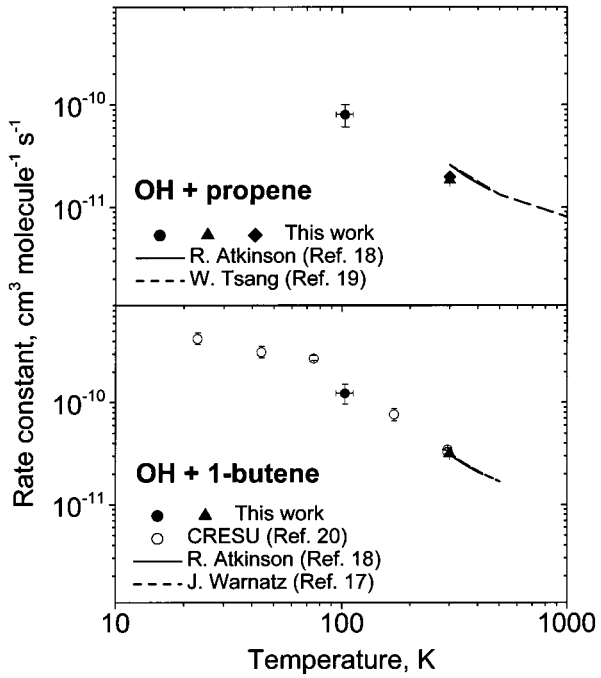

Figure 7. Rate constants of reactions (R1) and (R2) plotted as a function of temperature. Filled points show the results of the present measurements: filled circles are the low-temperature Laval nozzle expansion measurements, filled triangles and diamonds are the room-temperature measurements at total pressures of 1.5 and 5.5 Torr (200 and 733 Pa), respectively; open circles are the low-temperature data for reaction (R2) obtained in the CRESU apparatus;[24] lines represent the recommended high-temperature rate constants.[21-23]

recommended by Warnatz,[21] Atkinson,[22] and Tsang[23] on the log−log plots of k vs temperature. Figure 7 also presents the room-temperature ($T = 295$ K) rate constants of reactions (R1) and (R2) measured in this work. The rate constant for reaction (R2) measured at a total pressure of 1.5 Torr (200 Pa) is in excellent agreement with the recommended value, indicating that k_2 is in its high-pressure limit under our experimental conditions. The room-temperature rate constants of reaction (R1) measured at total pressures of 1.5 and 5.5 Torr (200 and 733 Pa, corresponding to total gas densities of 4.9×10^{16} and 1.8×10^{17} molecules cm^{-3}) make up 72% and 77% of the high-pressure rate constant value,[22,23] respectively, showing the importance of the falloff effects over this pressure range at $T = 295$ K. However, for the temperatures as low as 100 K, the falloff curve will be considerably shifted to lower pressures. Therefore, the rate constant of reaction (R1) measured at a similar total gas density (2.1×10^{16} molecules cm^{-3}) at $T = 103$ K can be expected to be essentially in its high-pressure limit.

The negative temperature dependence shown by the rate constants of reactions (R1) and (R2) is actually characteristic for the reactions of the OH radical with most alkenes.[22] A possible explanation of the inverse temperature dependence involves an assumption that the overall reaction rate is affected by formation of intermediate weakly bound complexes corresponding to minima existing along a complicated reaction coordinate, followed by competing backward and forward dissociation of these complexes.[22,35] Depending on relative heights of the barriers for forward and backward dissociation of the complex and the rigidities of the corresponding transition states, the overall rate constant may exhibit a negative temperature dependence.[36,37] However, recent ab initio calculations for OH + ethene reaction[38] show that the minimum energy path from the reagents to the addition product has neither barriers nor minima that could correspond to any intermediate complexes. In this case, the rate of reaction is determined by that of adiabatic capture on an electronic potential that monotonically decreases as the reagents approach one another, which may also lead to a negative temperature dependence of the rate constant.[39,40] Using the calculated potential energy surface and canonical variational transition state theory, Villa et al.[38] have reproduced the experimental negative temperature dependence of the OH + ethene reaction rate constant. Most likely, for the OH + propene and OH + 1-butene reactions, similar arguments are valid.

There is good agreement between the low-temperature Laval results for the reactions of OH radical with propene and 1-butene and the available literature data. This shows that our pulsed Laval nozzle apparatus with photolytic radical preparation is capable of providing an appropriate low-temperature environment for kinetic studies, as earlier demonstrated by the M. Smith group using a cold cathode discharge to form radicals.[14-16] Obviously, further work is required to evaluate more precisely the capabilities and limits of applicability of different methods used for low-temperature kinetic studies (certain discrepancies still exist in the low-temperature data obtained by different methods, e.g., for reactions OH + HBr,[16,20] $C_2H + C_2H_2$,[2,17,18,41] $C_2H + O_2$,[3,19,41] and OH + ethane[8,42]). Because many of the reactions of C_2H radical with unsaturated hydrocarbons have been studied at low temperatures by both the continuous Laval expansion method[41] and cryogenically cooled flow reactor,[2,3,5,7] these reactions could be good candidates for calibration reactions, necessary for further testing of the performance of the pulsed Laval nozzle technique. Kinetic experiments on reactions of OH, C_2H, and other hydrocarbon radicals are now in progress in our laboratory. Soon a series of new Laval nozzles will be fabricated, and the existing pumping system will be improved in order to significantly extend the range of experimental conditions (temperature and gas number density).

Finally, we would like to mention that reactions (R1) and (R2) are potentially important for the chemistry of Saturn's atmosphere, where the OH radical is one of the most important oxygen-containing transient species.[43,44] It is shown that the reactions of OH with saturated and unsaturated hydrocarbons are responsible for the photochemical production of organic compounds containing the C−O bond.[44] Recent models of Saturn's atmosphere include chemical and photochemical processes that involve hydrocarbon species containing up to six carbon atoms;[45] therefore, the information on the low-temperature kinetics of the reactions of OH with propene and 1-butene may be essential for those studies.

The authors are grateful to A. R. Ravishankara and D. C. McCabe (NOAA Aeronomy Laboratory, Boulder, CO) for providing a sample of concentrated hydrogen peroxide and for stimulating discussions. We also thank M. A. Smith at the University of Arizona for the program code for Laval nozzle design. The support of this research by the National Aeronautics and Space Administration (Grant No. NAG5-8923) is gratefully acknowledged.

References and Notes

(1) Sims, I. R.; Smith, I. W. M. *Annu. Rev. Phys. Chem.* **1995**, *46*, 109.
(2) Pedersen, J. O. P.; Opansky, B. J.; Leone, S. R. *J. Phys. Chem.* **1993**, *97*, 6822.
(3) Opansky, B. J.; Seakins, P. W.; Pedersen, J. O. P.; Leone, S. R. *J. Phys. Chem.* **1993**, *97*, 8583.
(4) Opansky, B. J.; Leone, S. R. *J. Phys. Chem.* **1996**, *100*, 4888.
(5) Opansky, B. J.; Leone, S. R. *J. Phys. Chem.* **1996**, *100*, 19 904.
(6) Hoobler, R. J.; Opansky, B. J.; Leone, S. R. *J. Phys. Chem. A* **1997**, *101*, 1338.
(7) Hoobler, R. J.; Leone, S. R. *J. Phys. Chem. A* **1999**, *103*, 1342.
(8) Clarke, J. S.; Kroll, J. H.; Donahue, N. M.; Anderson, J. G. *J. Phys. Chem. A* **1998**, *102*, 9847.
(9) Rowe, B. R.; Dupeyart, G.; Marquette, J. B.; Gaucherel, P. *J. Chem. Phys.* **1984**, *80*, 4915.
(10) Dupeyart, G.; Marquette, J. B.; Rowe, B. R. *Physics of Fluids* **1985**, *28*, 1273.
(11) Sims, I. R.; Queffelec, J.-L.; Defrance, A.; Rebrion-Rowe, C.; Travers, D.; Bocherel, P.; Rowe, B. R.; Smith, I. W. M. *J. Chem. Phys.* **1994**, *100*, 4229.
(12) James, P. L.; Sims, I. R.; Smith, I. W. M.; Alexander, M. H.; Yang, M. B. *J. Chem. Phys.* **1998**, *109*, 3882.
(13) Smith, I. W. M.; Rowe, B. R. *Accounts Chem. Res.* **2000**, *33*, 261.
(14) Atkinson, D. B.; Smith, M. A. *Rev. Sci. Instrum.* **1995**, *66*, 4434.
(15) Atkinson, D. B.; Smith, M. A. *J. Phys. Chem.* **1994**, *98*, 5797.
(16) Atkinson, D. B.; Jaramillo, V. I.; Smith, M. A. *J. Phys. Chem. A* **1997**, *101*, 3356.
(17) Lee, S.; Hoobler, R. J.; Leone, S. R. *Rev. Sci. Instrum.* **2000**, *71*, 1816.
(18) Lee, S.; Samuels, D. A.; Hoobler, R. J.; Leone, S. R. *J. Geophys. Res.-Planets* **2000**, *105*, 15 085.
(19) Lee, S.; Leone, S. R. *Chem. Phys. Lett.* **2000**, *329*, 443.
(20) Sims, I. R.; Smith, I. W. M.; Clary, D. C.; Bocherel, P.; Rowe, B. R. *J. Chem. Phys.* **1994**, *101*, 1748.
(21) Warnatz, J. Rate Coefficients in the C/H/O system. In *Combustion Chemistry*; Gardiner, W. C., Jr., Ed.; Springer-Verlag: New York, 1984.
(22) Atkinson, R. *Chem. Rev.* **1986**, *86*, 69.
(23) Tsang, W. *J. Phys. Chem. Ref. Data* **1991**, *20*, 221.
(24) Sims, I. R.; Smith, I. W. M.; Bocherel, P.; Defrance, A.; Travers, D.; Rowe, B. R. *J. Chem. Soc.-Faraday Trans.* **1994**, *90*, 1473.
(25) Chidsey, I. L.; Crosley, D. R. *J. Quant. Spectrosc. Radiat. Transf.* **1980**, *23*, 187.
(26) Coxon, J. A. *Can. J. Phys.* **1980**, *58*, 933.
(27) Luntz, A. C. *J. Chem. Phys.* **1980**, *73*, 1143.
(28) Park, C. R.; Wiesenfeld, J. R. *J. Chem. Phys.* **1991**, *95*, 8166.
(29) Gericke, K. H.; Klee, S.; Comes, F. J.; Dixon, R. N. *J. Chem. Phys.* **1986**, *85*, 4463.
(30) Germann, G. J.; Valentini, J. J. *Chem. Phys. Lett.* **1989**, *157*, 51.
(31) Atkinson, R.; Baulch, D. L.; Cox, R. A.; Hampson, R. F.; Kerr, J. A.; Rossi, M. J.; Troe, J. *J. Phys. Chem. Ref. Data* **1997**, *26*, 521.
(32) Kliner, D. A. V.; Farrow, R. L. *J. Chem. Phys.* **1999**, *110*, 412.
(33) Baulch, D. L.; Cobos, C. J.; Cox, R. A.; Esser, C.; Frank, P.; Just, T.; Kerr, J. A.; Pilling, M. J.; Troe, J.; Walker, R. W.; Warnatz, J. *J. Phys. Chem. Ref. Data* **1992**, *21*, 411.
(34) Taylor, B. N.; Kuyatt, C. E. *Guidelines for Evaluating and Expressing the Uncertainty of NIST Measurement Results, NIST Technical Note 1297*; US Government Printing Office: Washington, D. C., 1994.
(35) Abbatt, J. P. D.; Anderson, J. G. *J. Phys. Chem.* **1991**, *95*, 2382.
(36) Mozurkewich, M.; Benson, S. W. *J. Phys. Chem.* **1984**, *88*, 6429.
(37) Troe, J. *J. Chem. Soc.-Faraday Trans.* **1994**, *90*, 2303.
(38) Villa, J.; Gonzalez-Lafont, A.; Lluch, J. M.; Corchado, J. C.; Espinosa-Garcia, J. *J. Chem. Phys.* **1997**, *107*, 7266.
(39) Clary, D. C. *Annu. Rev. Phys. Chem.* **1990**, *41*, 61.
(40) Smith, I. W. M. *Int. J. Mass Spectom. Ion Process.* **1995**, *150*, 231.
(41) Chastaing, D.; James, P. L.; Sims, I. R.; Smith, I. W. M. *Faraday Discuss.* **1998**, 165.
(42) Sharkey, P.; Smith, I. W. M. *J. Chem. Soc.-Faraday Trans.* **1993**, *89*, 631.
(43) Ollivier, J. L.; Dobrijevic, M.; Parisot, J. P. *Planet Space Sci.* **2000**, *48*, 699.
(44) Moses, J. I.; Lellouch, E.; Bezard, B.; Gladstone, G. R.; Feuchtgruber, H.; Allen, M. *Icarus* **2000**, *145*, 166.
(45) Moses, J. I.; Bezard, B.; Lellouch, E.; Gladstone, G. R.; Feuchtgruber, H.; Allen, M. *Icarus* **2000**, *143*, 244.